This is the Pre-Published Version.

S. Lin, X. Huang (2022) *Extinction of Wood Fire: Modeling Smoldering and Near-Limit Flame under Irradiation*, **Fire Technology**, https://doi.org/10.1007/s10694-022-01295-2

Extinction of Wood Fire: Modeling Smoldering and Near-Limit Flame under Irradiation

Shaorun Lin[a,b] and Xinyan Huang[a,*]

[a] *Research Centre for Fire Safety Engineering, Department of Building Environment and Energy Engineering, The Hong Kong Polytechnic University, Kowloon, Hong Kong*

[b] *The Hong Kong Polytechnic University Shenzhen Research Institute, Shenzhen, China*

*Corresponding to xy.huang@polyu.edu.hk (X. Huang)

Abstract: Timber, as renewable and carbon-neutral construction material, has gained a new renaissance for tall buildings to meet the initiatives of sustainable construction, but their fire safety is still a major concern. Previously, we identified a unique combustion mode showing a near-limit flame that is weak, blue, discrete and tends to attach to the hot smoldering wood residue surface. Such a flame is an intermediate combustion mode between the typical yellow wood flame and pure smoldering and occurs when the irradiation is above 40 kW/m^2. This work proposes two numerical models based on the open-source code Gpyro and FDS to reproduce the solid-phase smoldering and the gas-phase near-limit flame, respectively. The solid-phase model demonstrates that the gaseous fuels for the near-limit flame mainly come from the pyrolysis of lignin that is maintained by the heat evolved from the internal char oxidation and external heating. The gas-phase model demonstrates the necessity of a hot surface and a small critical mass flux to maintain a near-limit flame that has a limited buoyancy effect. Finally, different flame regimes are obtained by the numerical simulations and summarized as a function of the fuel surface temperature and gaseous fuel mass flux. This is the first time that comprehensive models have been used to reveal the underlying mechanisms for smoldering-assisted flame, so it provides a better understanding of fire dynamics and helps evaluate the fire risk of timber under real fire scenarios.

Keywords*: Wood fire; Extinction limit; Fire modeling; Fire safety; charring material.*

Graphic Abstract

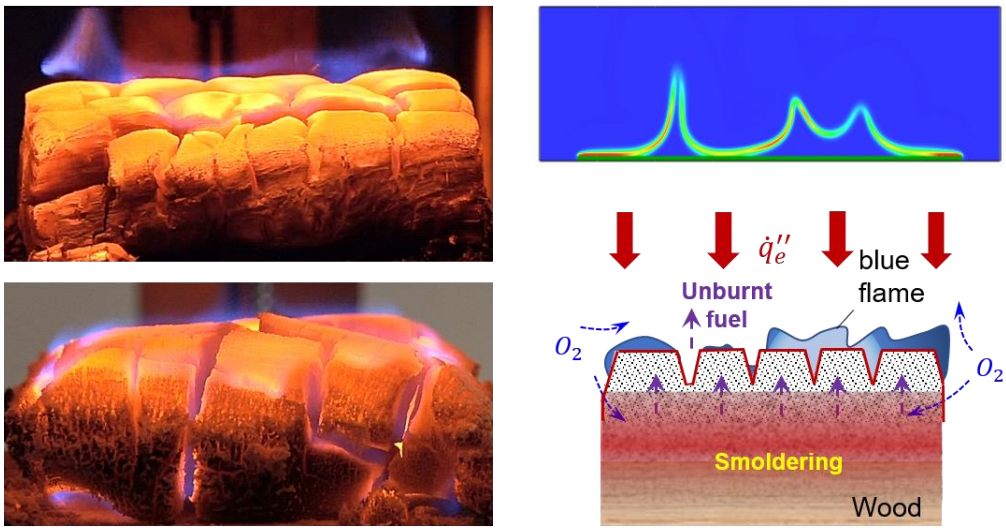

Nomenclature

Symbols		***Greeks***	
c_p	specific heat capacity (J/kg·K)	δ	thickness (m)
D	diffusivity (m^2/s)	v	stochiometric coefficient (-)
E	activation energy (kJ/mol)	ρ	density (kg/m^3)
g	oxidation function	ψ	Porosity (-)
h	enthalpy (J/kg)	$\dot{\omega}'''$	volumetric reaction rate (g/m^3·s)
h_c	convective coefficient (W/m^2·s)	***Subscripts***	
h_m	mass transfer coefficient (g/m^2·s)	0	initial
ΔH	heat of reaction (J/kg)	A	species A
k	thermal conductivity (W/m·K)	B	blue flame
K	permeability (m^2)	crt	critical
m	mass (kg)	e	external heating
$\dot{m}''$	mass flux (kg/m^2·s)	ex	extinction
n	reaction order	F	fuel
P	pressure (Pa)	g	gas
$\dot{q}''$	heat flux (kW/m^2)	i	condensed species number
R	universal gas constant (J/mol·K)	ig	ignition
t	time (s)	k	reaction number
T	temperature (°C)	O_2	oxygen
TGA	Thermogravimetric analysis	r	radiation
Y	mass fraction	s	surface
Z	pre-exponential factor (s^{-1})	Y	yellow flame

1. Introduction

Timber has gained a new renaissance as a favored construction material for high-rise buildings that may pave a way for future carbon-neutral construction [1, 2]. In recent years, many green high-rise timber buildings have sprung up rapidly all around the world, but the fire risk or flammable nature of timber has led to strict fire safety and structural requirements that increase its cost and limit its popularity. From the Notre-Dame de Paris fire in 2019 (Fig. 1a) to the Austria Top Mountain Crosspoint Motorcycle Museum fire in 2021 (Fig. 1b), both historic and modern wooden structures were ravaged by fires, which re-push the fire safety of timber buildings to be a public concern [3]. Thus, it is urgent to fully understand the fire dynamics and combustion limits of wood materials to guide the fire safety design of timber structures.

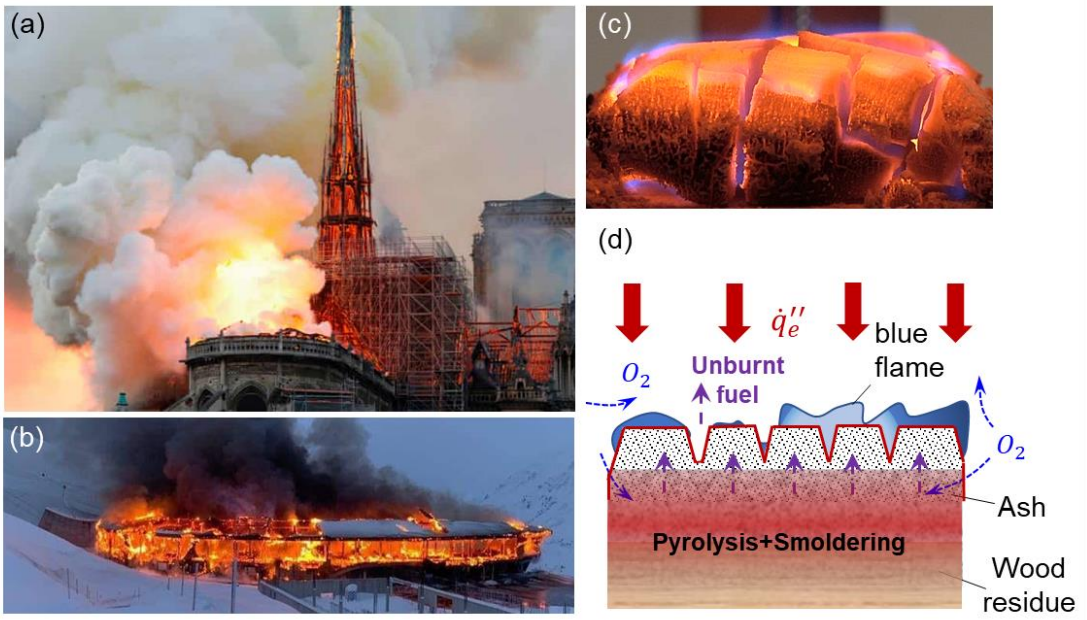

Fig. 1. Examples of huge fires in timber structures: (a) the Notre-Dame de Paris fire in 2019 (Photo courtesy Francois Guillot) and (b) the Austria Top Mountain Crosspoint Motorcycle Museum fire in 2021 (Photo courtesy Alex Strange), and (c) the photo as well as (d) schematic diagram of the near-limit blue flame above the hot smoldering surface (Video S1) [3].

In the literature, various wooden materials have been studied extensively to understand the flame initiation and subsequent propagation of timber building fires [4–12]. Without strong irradiation, the flame is sometimes not able to sustain above the timber material after ignition, i.e., self-extinction may occur [3, 13–15]. In recent years, the self-extinction of timber flame has become a hot research topic and is believed to be a crucial concept that supports the fire safety of high-rise timber buildings. For the most natural and engineered woods, the minimum mass flux and heat flux for flameout are relatively constant at 4 g/m^2-s and 40 kW/m^2, respectively [14]. Nevertheless, flame extinction is not the end of a fire, as it may sustain as a smoldering fire which could lead to a fatal condition because of a larger emission factor of CO [16].

In our previous work [3], a unique near-limit flame (Fig.1c, Fig.1d and Video S1) that sustained above a hot smoldering wood surface was observed and existed for more than 30 min. Such a near-limit flame was weak, blue, and discrete that tended to attach to the fuel residue surface, different from the normal buoyancy-raised sooty yellow flame. A similar near-limit flame was also observed on the glowing charcoal and incense [17, 18]. If the irradiation was smaller than 40 kW/m^2, the yellow wood flame extinguished at the mass flux of about 4 g/m^2·s and transitioned directly to smoldering. However, when the irradiation was larger than 40 kW/m^2, the yellow flame transitioned to the blue flame that did not extinguish until the mass flux of around 1 g/m^2·s, extending the conventional flame extinction limit (4 g/m^2·s) of wood materials. As the discrete blue flame only partially covered the char surface, the oxygen molecules may diffuse into the cracked and porous char layer to maintain the char oxidation

that releases heat to sustain the in-depth pyrolysis which was demonstrated by the emissions measured in our previous experiments [3].

Our experiments also found that the near-limit blue flame appeared only if the char surface temperature exceeded 700 ℃ [3]. Therefore, theoretical analysis hypothesized two critical conditions for this near-limit flame,

(I) In-depth pyrolysis (mainly lignin) is sustained by the internal smoldering combustion and external heating to provide flammable gases, and

(II) Hot surface is maintained by large external radiation to extend the lower flammability limit [3].

So far, these two hypotheses have not been verified by a physics-based numerical model.

Numerical simulation of wood fires is an emerging topic, and many multi-scale numerical simulations have investigated the processes of wood pyrolysis [1, 19], deformation [20], flaming ignition [21], smoldering ignition [22], and flame spread [23]. The influencing factors including fuel properties [21], chemical kinetics [24], oxygen supply [25], and irradiation [26] were also explored, which laid a solid foundation for simulating both smoldering and flaming wood fires.

This work establishes a numerical framework to verify the aforementioned two hypotheses for the near-limit flame above a hot smoldering surface. The solid-phase model is constructed based on an open-source code Gpyro [27] to demonstrate the fuels for this special flame behavior is a long-lasting small fuel mass flux from high-temperature pyrolysis reaction (mainly lignin) maintained by internal smoldering combustion and external heating. Then, a gas-phase DNS model has been constructed to demonstrate the necessity of a hot surface and a small critical mass flux to main a near-limit flame that is discontinuous and weakly affected by buoyancy. Finally, different flame regimes as a function of the fuel surface temperature and gaseous fuel mass flux are also quantified.

2. Computational model

As the simulation of our past experiments [3] is the starting point of the present study, a brief introduction to the experimental details is firstly given here. All experiments were conducted under the cone calorimeter (FTT iCone Plus). The conical heater could provide relatively constant and uniform irradiation ($\dot{q}_e''$) to the top surface of the wood sample. Once the flame was piloted by the spark, external heating was continued until the sample mass no longer changed or it completely turned into white ashes (i.e., burnout). The test process was recorded by a camera, and the sample mass was monitored by the precision scale (± 0.1 mg). The surface temperature of wood was carefully measured using two K-type thermocouples (0.5 mm junction bead diameter) that were closely contacted with the wood top surface. In total, six different types of natural woods were tested, which have the same dimension of 10 cm × 10 cm × 3 cm and different densities. All wood samples were fully dried at 90 ºC before the tests. More descriptions of experimental details can be found in [3].

2.1 Solid-phase model

In general, as a natural biomass fuel, wood has three major components with different pyrolysis temperatures, namely hemicellulose (~250 ℃), cellulose (~300 ℃), and lignin (~350 ℃) [28, 29], and their pyrolysis processes can be expressed by a 3-step pyrolysis kinetic scheme (Eq. 1-3).

$$\text{Hemicellulose} \rightarrow \text{Char} + \text{Pyrolyzates} \quad [\text{hp}] \quad (1)$$

$$\text{Cellulose} \rightarrow \text{Char} + \text{Pyrolyzates} \quad [\text{cp}] \quad (2)$$

$$\text{Lignin} \rightarrow \text{Char} + \text{Pyrolyzates} \quad [\text{lp}] \quad (3)$$

$$\text{Char} + O_2 \rightarrow \text{Ash} + \text{gases} \quad [\text{co}] \quad (4)$$

For modeling smoldering combustion, char oxidation (Eq. 4) has to be included in the model, which is responsible for the second major peak in the TGA curve (see Fig. A1). The balance between complexity and accuracy of the biomass kinetics in the mesoscale modeling has been explored in [28], which is not further discussed here. Note that the wood will be dried before the occurrence of heterogeneous reactions, thus the drying process (*dr*) is also included in our model as

$$\text{Water} \rightarrow \text{Water vapor} \quad [\text{dr}] \quad (5)$$

To model the smoldering reactions (1-step drying, 3-step pyrolysis, and 1-step char oxidation), the destruction rate of the condensed species A in reaction k is expressed using Arrhenius law as

$$\dot{\omega}'''_{dA_k} = \frac{\left(\bar{\rho} Y_{A_k} \Delta z\right)_\Sigma}{\Delta z} Z_k \, exp\left(-\frac{E_k}{RT}\right)\left(\frac{\bar{\rho} Y_{A_k} \Delta z}{\left(\bar{\rho} Y_{A_k} \Delta z\right)_\Sigma}\right)^{n_k} Y_{O_2}^{n_{O_2,k}} \quad (6)$$

$$\left(\bar{\rho} Y_i \Delta z\right)_\Sigma \equiv \left(\bar{\rho} Y_i \Delta z\right)|_{t=0} + \int_0^t \dot{\omega}'''_{fi}(\tau) \Delta z(\tau) d\tau \quad (7)$$

where Z_k is the pre-exponential factor, and E_k is the activation energy. The kinetic parameters for the smoldering of wood are obtained by optimizing the TG data in both inert and oxidative atmospheres using the Genetic Algorithm (see detailed description in [19, 30]) and the results are listed in Table 1 and Fig. A1.

To better explain the experiment and understand the role of different wood components and smoldering reactions, a 1-D numerical model (see Fig. 2a) based on an open-source code Gpyro [27] is applied here. Previously, this model has successfully simulated the pyrolysis and smoldering of wood [21, 25], peat [31, 32] and other biomass fuels. Details of Gpyro can be found in [27], thus only the governing conservation equations are provided here, including the conservation of mass (Eq. 8), species (Eq. 9) and energy (Eq. 10) in the condensed phase as well as the mass (Eq. 11), species (Eq. 12), and momentum (Darcy's law) (Eq. 13) in the gas phase. The details of the mathematical forms of these equations and the definitions of all symbols can also be found in the *Nomenclature* or in [27].

$$\frac{\partial \bar{\rho}}{\partial t} = -\dot{\omega}'''_{fg} \quad (8)$$

$$\frac{\partial(\bar{\rho}Y_i)}{\partial t} = \dot{\omega}'''_{fi} - \dot{\omega}'''_{di} \tag{9}$$

$$\frac{\partial(\bar{\rho}\bar{h})}{\partial t} + \frac{\partial(\dot{m}''\bar{h}_g)}{\partial z} = \frac{\partial}{\partial z}\left(\bar{k}\frac{\partial T}{\partial z}\right) + \sum_{k=1}^{K}\dot{\omega}'''_k \Delta H_k \tag{10}$$

$$\frac{\partial(\rho_g\bar{\psi})}{\partial t} + \frac{\partial\dot{m}''}{\partial z} = \dot{\omega}'''_{fg} \tag{11}$$

$$\frac{\partial(\rho_g\bar{\psi}Y_j)}{\partial t} + \frac{\partial(\dot{m}''Y_j)}{\partial z} = -\frac{\partial}{\partial z}\left(\rho_g\bar{\psi}D\frac{\partial Y_j}{\partial z}\right) + \dot{\omega}'''_{k,j} \tag{12}$$

$$\dot{m}'' = -\frac{\bar{K}}{\nu}\frac{\partial P}{\partial z} \qquad \left(P = \rho_g R_s T\right) \tag{13}$$

Table 1. Chemical kinetic parameters and yields of 5-step reactions for the wood, where ΔH>0 is endothermic and ΔH<0 is exothermic.

	dr	*hp*	*cp*	lp	co
$\lg Z_k$ ($\lg(s^{-1})$)	17	8.2	11.4	21.4	12.9
E_k (kJ/mol)	130	106	154	229	184
n_k (-)	1	1.49	1.21	8.1	1.27
n_{k,O_2} (-)	0	0	0	0	1
$v_{B,k}$ (kg/kg)	0	0.24	0.27	0.40	0.06
ΔH_k (MJ/kg)	2.26	0.2	0.2	0.2	-20
$v_{O_2,k}$ (kg/kg)	0	0.5	0.5	0.5	1.5

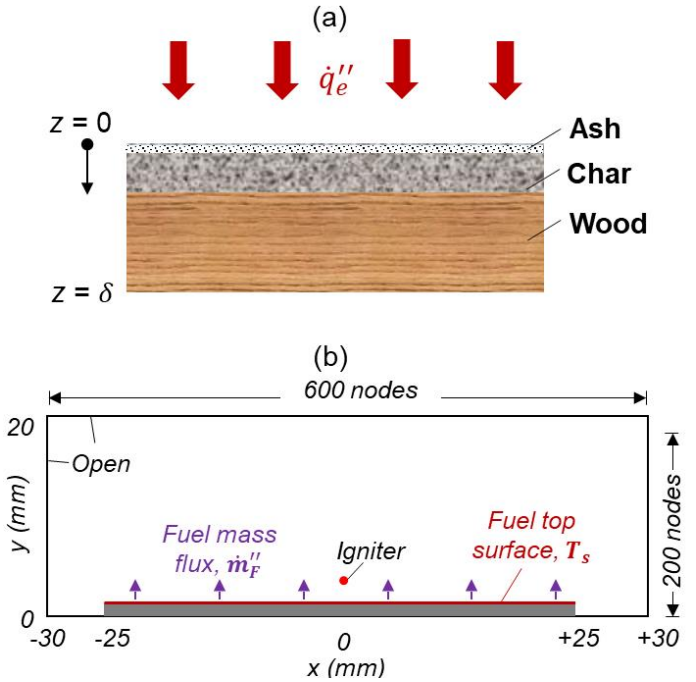

Fig. 2. Schematic diagrams of (a) solid-phase and (b) gas-phase computational domains.

The 1-D solid-phase model assumes the thermal equilibrium between gas and solid phase, unit Schmidt number, and the same gas diffusion coefficient and specific heat for all gas species. The averaged properties in each cell are calculated using the appropriate mass fraction or volume fraction. The detailed species thermophysical properties and kinetic parameters can be found in [21] and Table 2. The sample height is equal to the sum of the heights of each cell. Simulations were performed with an initial cell size of 0.1 mm and an initial time step of 0.02 s. Reducing the cell size and time step by a factor of two results in no significant difference, so this discretization is proper.

Table 2. Physical parameters of condensed-phase species, ρ (bulk density), k (thermal conductivity), and c (specific heat) [21, 33], where k and c increase with temperature.

Species	Y_0	ρ	k	c
water	0.08	1000	0.6	4200
hemicellulos	0.19	711	0.2	1500
cellulose	0.49	630	0.2	1500
lignin	0.24	413	0.2	1500
char	0	250	0.05	3000
ash	0	15	0.05	3000

The 1-D computational domain has the same sample thickness (δ=30 mm) as that in the experiment [3]. Based on the experimental measurement [27], the ignition criterion uses a critical mass flux of 10 g/m^2·s. At the top free surface ($z = 0$), before ignition, the constant irradiation is set to be the same as the cone heater, as well as an environmental convective cooling coefficient h_c =10 W/m2·K and the surface re-radiation. After ignition, the constant flame heat flux of 20 kW/m^2 is added in addition to the irradiation from the cone heater [34]. Once the total mass flux is below 4 g/m^2·s, the flame heat flux is removed (due to the extinction of strong yellow flame [3]), and the oxygen diffusion boundary is applied. It is difficult for oxygen to diffuse into the low-porous wood and char, so a small mass transfer number, $h_m = 0.1$ g/m^2·s, is used for gas species conservation (see Fig. 2a).

At the bottom boundary (z = 30 mm), a cooling coefficient is set to 5 W/m^2·K to simulate the bottom heat loss, and there is no mass flux. The ambient pressure and temperature are constant at 1 atm and 300 K, respectively. The numerical stability and discretization are verified previously [21, 25, 31].

2.2 Gas-phase model

To better understand the effects of mass flux and surface temperature on flame behaviors in charring materials, a simplified gas-phase numerical model is also adopted to reproduce the near-limit flame and verify the reason for its formation. As the first approximation, the 2-D model is established to save computational cost, and the computational domain is 20 mm × 60 mm (Fig. 2b). A planar Cartesian coordinate shows the geometric position in horizontal (x) and vertical (y) directions. This work uses the Fire Dynamics Simulator (FDS 6.7.0) [35] to establish the model and its DNS solver to calculate

the finite-rate flame chemistry. The convergence study suggests that a uniform grid with Δl = 0.3 mm or smaller can effectively resolute the flame with the 1-step finite-rate chemistry. To ensure the computational accuracy, a mesh resolution of Δl = 0.1 mm is adopted with 600 transverse nodes from x = -30 to 30 mm, and 200 streamwise nodes from y = 0 to 20 mm. Thus, the total number of mesh is 1.2×10^5.

Although the exact emission composition from the smoldering wood is complex (e.g., CO, CO_2, CH_4, C_2H_4, H_2, C_2H_6, and C_n (n≥3)), hydrocarbons are considered as the main fuel component of pyrolysis products [36, 37]. Therefore, as a first approximation, this model uses the 1-step finite-rate flame chemistry, and the chemical formula of propane (C_3H_8) is used to represent the fuel gas. Kinetic parameters include the pre-exponential factor of $Z = 1.2\times10^{16}$ (mol/m^3)·s^{-1}, the activation energy of E_a = 100 kJ/mol, 1st-order reaction for both fuel and oxygen, and the heat of combustion of ΔH = 20 MJ/kg (measured from cone calorimeter) [38]. Note that the Arrhenius equation applied in FDS is a special case of the more generalized form (Eq. 6) in Gpyro [39] with $n_{O_2,k} = 0$, $(\bar{\rho}Y_i\Delta z)_\Sigma$ replaced by $(\bar{\rho}\Delta z)|_{t=0}$, and no volume change ($\Delta z = constant$). Therefore, the Arrhenius equation in FDS could be expressed as

$$\dot{\omega}'''_{dA_k} = \bar{\rho}|_{t=0} Z_k \, exp\left(-\frac{E_k}{RT}\right)\left(\frac{\bar{\rho}Y_{A_k}}{\bar{\rho}|_{t=0}}\right)^{n_k} \tag{14}$$

The temperature-related viscosity and diffusivity of propane are set for fuel gas. Only the fuel top surface is included in the model, and the sample center coincides with the coordinate origin (Fig. 2b).

The heterogeneous reactions in the solid fuel are not explicitly solved in this model, because the emission gas composition could not be determined, and the numerical model would become too complex to identify the primary parameter for the near-limit flame. Thus, the intensity is simply controlled by the gaseous fuel mass flux on the surface. For simplicity, the external radiation is also not resolved in the model. Instead, a fuel surface temperature is set based on a monotonical correlation with external radiation [3].

As implied from the previous experiment [3], two key parameters are controlled in the simulation, (1) the fuel top surface temperature, T_s, and (2) the fuel mass flux, $\dot{m}''$. The bottom boundary is set to room temperature, and the top and side boundaries are open. At time zero, the fuel gas is released from the solid surface with the same temperature by assuming the Stefan flow and solid-gas thermal equilibrium. To pilot a flame, like a spark in the experiment, a hot igniter of a single mesh with a temperature of 1400 °C is placed 5 mm above the surface for 1.4 s. Afterward, the igniter is removed, and the flame can stabilize itself under free convection. The initial temperature of 25 °C and the pressure of 1 atm are set for the domain.

3. Results and discussion

3.1 Modeling of smoldering

Fig. 3 shows the modeled mass loss of each species and the overall mass-loss flux of bench-scale wood samples under the external radiation of (a) 30 kW/m^2 and (b) 60 kW/m^2. For more detailed solid-phase modeling results, see Videos S2. The modeling results are also compared with the corresponding experimental data [3]. In general, considering the complex nature of the combustion process, a satisfactory agreement between computational predictions and experimental data could be observed [3], and the difference between experiment and simulation is comparable to the uncertainty between repeating tests. Therefore, the accuracy of our model is validated.

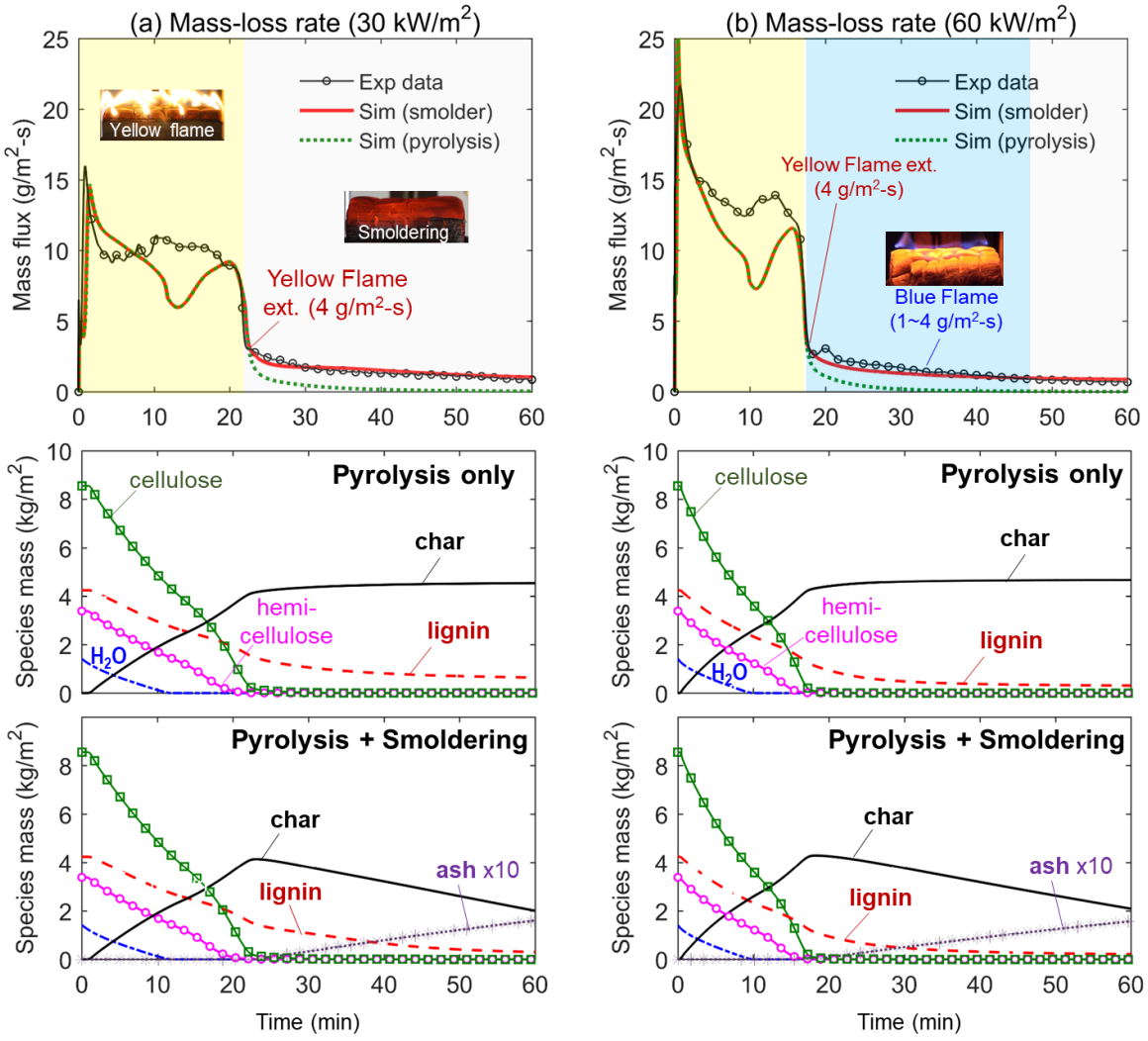

Fig. 3. Comparison between modeled and experimental mass-loss rate and the evolution of modeled species under the external radiation of (a) 30 kW/m^2 and (b) 60 kW/m^2.

On the other hand, by including the smoldering (i.e., char oxidation) process in the model, both the mass-loss rate before and after the extinction of yellow flame ($\dot{m}'' < 4$ g/m^2·s) can also be well predicted (Fig. 3), where the decomposition of lignin is accelerated due to the extra heat from char

oxidation. For better observation, the detailed heterogeneous reaction profiles are also shown in Fig. 4. Clearly, both Figs. 3 and 4 demonstrate that the mass loss after the strong yellow flame is mainly caused by both the oxidation of char (Eq. 4) and the pyrolysis of lignin (Eq. 3). After a strong yellow flame, the pyrolysis of lignin can continue to produce a sufficient mass flow of gaseous fuels to support a lean flame on the surface. In order to promote the decomposition of lignin inside the wood, a high temperature (> 500 °C) is required, which can only be sustained by robust exothermic char oxidation together with larger external heating. Therefore, we can confirm that it is essential to have in-depth smoldering combustion of wood to promote the pyrolysis of lignin and maintain the gaseous fuel flux to the wood residue surface to support a near-limit flame.

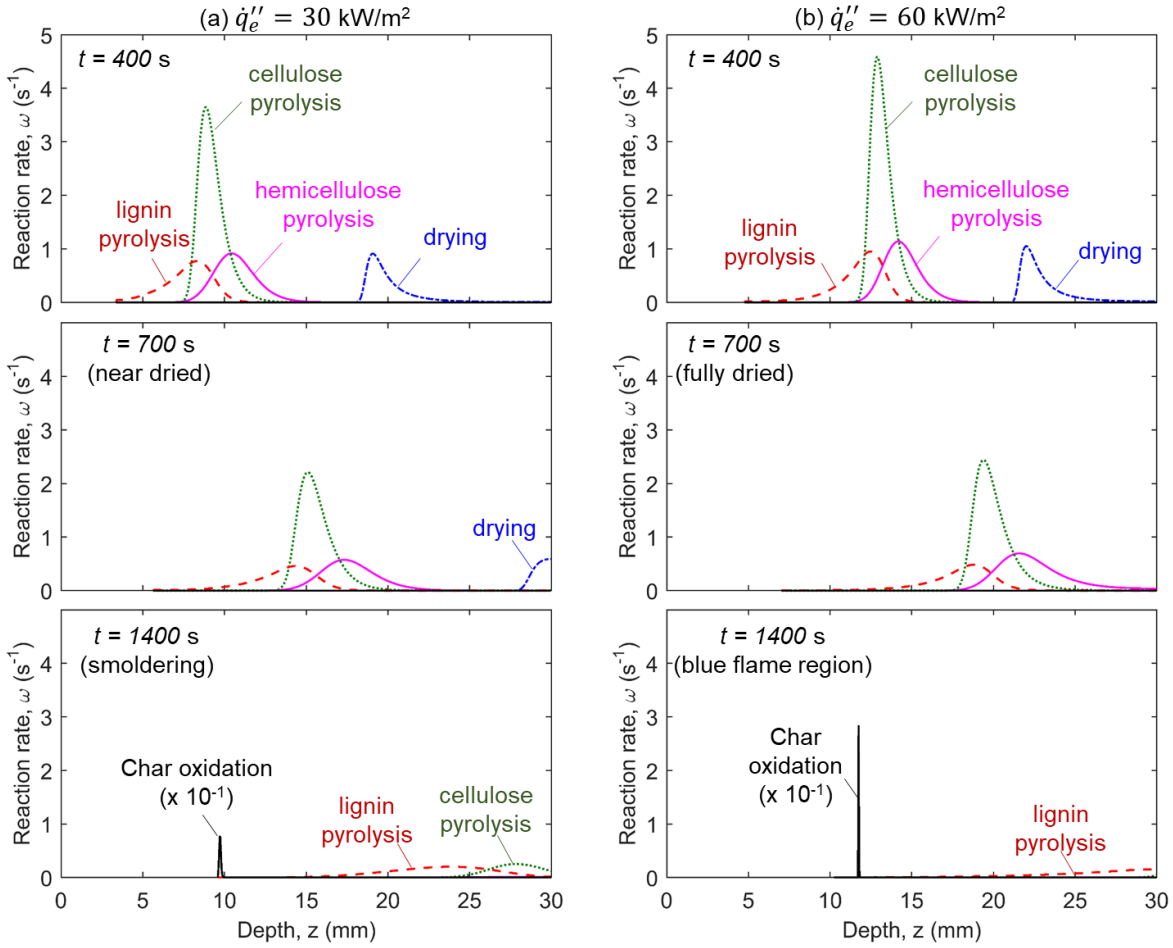

Fig. 4. Modeled 5-step heterogeneous reaction at different smoldering stages under irradiation of (a) 30 kW/m^2 and (b) 60 kW/m^2 (see Video S2).

Fig. 5(a) further shows the predicted time evolutions of surface temperatures of the same cases in Figs. 3 and 4, where the experimental data are plotted for comparison as well. Once the irradiation is applied, the top surface temperature dramatically increases and eventually approaches the quasi-steady state by balancing the heat loss. In general, the predictions agree well with our experimental measurement [3], and our model is further validated. Fig. 5(b) also summarized the steady surface

temperature under different external heating scenarios, where the temperature increases as the external irradiation level increases. In the experiments, we found that the near-limit blue flame may survive only when the surface temperature is sufficiently high, that is, $T_s > T_B \approx 700$ °C at $\dot{q}_e'' > \dot{q}_B'' \approx 40$ kW/m^2. Therefore, the wood surface temperature may be an important factor that affects the formation of near-limit blue flame, which will be further verified in the gas-phase simulation.

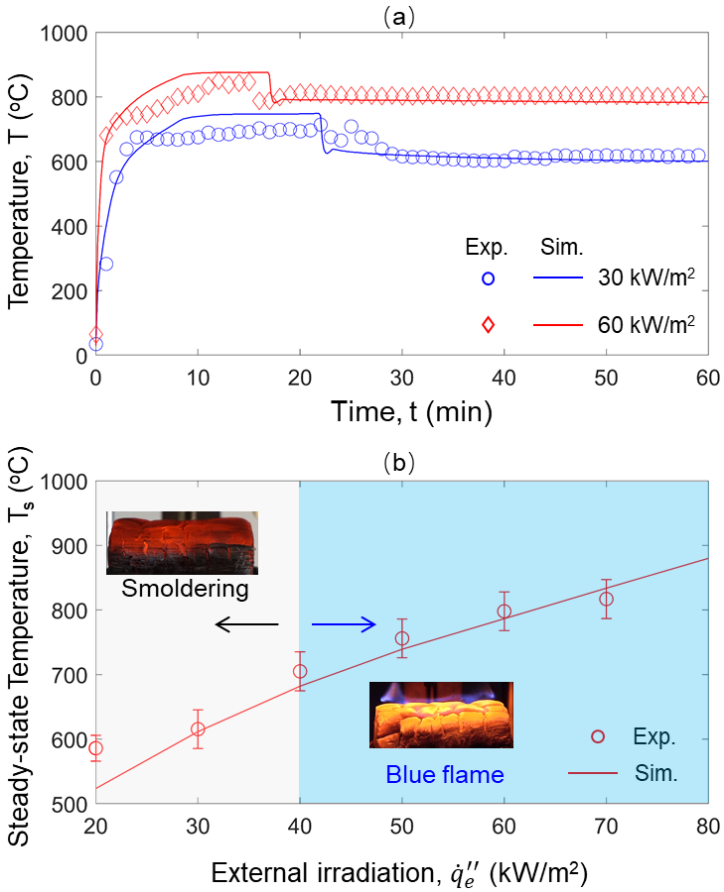

Fig. 5. Experimental and computational results of (a) evolution of top surface temperature, and (b) steady-state temperature as a function of external irradiation.

3.2 Modeling the near-limit flame

Fig. 6 shows the modeled flame shape and heat release rate of various fuel surface temperatures (T_s) and gaseous fuel mass flux ($\dot{m}_F''$) at several moments (also see Video S3). With $T_s = 600$ °C, $\dot{m}_F'' = 0.5$ g/m^2·s (Fig. 6a), the autoignition on the surface can be observed, and once ignited, the premixed flame propagates on the hot surface. Because the fuel gas is limited, the premixed flame is expected to be fuel-lean, which supports the appearance of the near-limit flame. The observed flame shape and behaviors agree with the late-stage surface flame in the experiment [3]. The autoignition is periodic, and its average frequency reduces with the decreasing fuel mass flux. Eventually, at $\dot{m}_F'' = 0.3$ g/m^2·s (Fig. 6b), the heat release rate becomes too weak to support a flame, and only a hot plume is observed, that is, flame extinction.

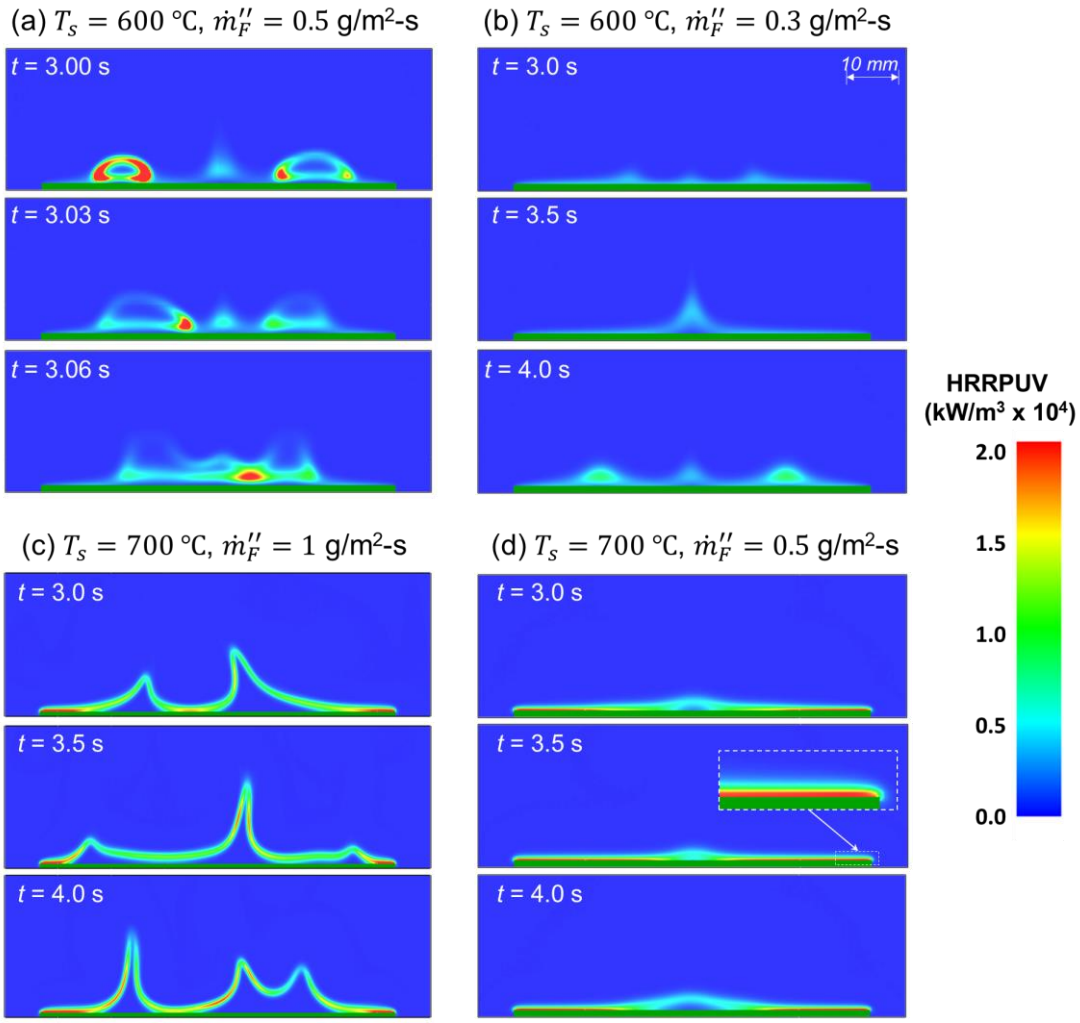

Fig. 6. Modeled flame shape and heat release rate (a) $T_s = 600$ °C, $\dot{m}''_F = 0.5$ g/m²·s, (b) $T_s = 600$ °C, $\dot{m}''_F = 0.3$ g/m²·s, (c) $T_s = 700$ °C, $\dot{m}''_F = 1$ g/m²·s, and (d) $T_s = 700$ °C, $\dot{m}''_F = 0.5$ g/m²·s (see Video S3).

By increasing either the fuel surface temperature or the gaseous fuel mass flux, the continual autoignition processes on the hot surface eventually disappear, while a continuous flame sheet can be observed (Fig. 6c). Nevertheless, there are several separate flame peaks, which match the early-stage surface flame observed in the experiment [3]. Further increasing the fuel mass flux, a single flame with only one peak will be observed, like the regular yellow wood flame. The flame height increases with the fuel mass flux (Fig. 7a), behaving like the classical laminar gaseous jet diffusion flame. On the other hand, when the surface temperature is very high while the gaseous fuel mass flux is very low (Fig. 6d), all the fuel will be consumed within 1 mm above the fuel surface, and the effect of buoyancy is negligible. This behavior is also observed in the very late stage of surface flame before it transitions to smoldering [3] (see Fig. 1c).

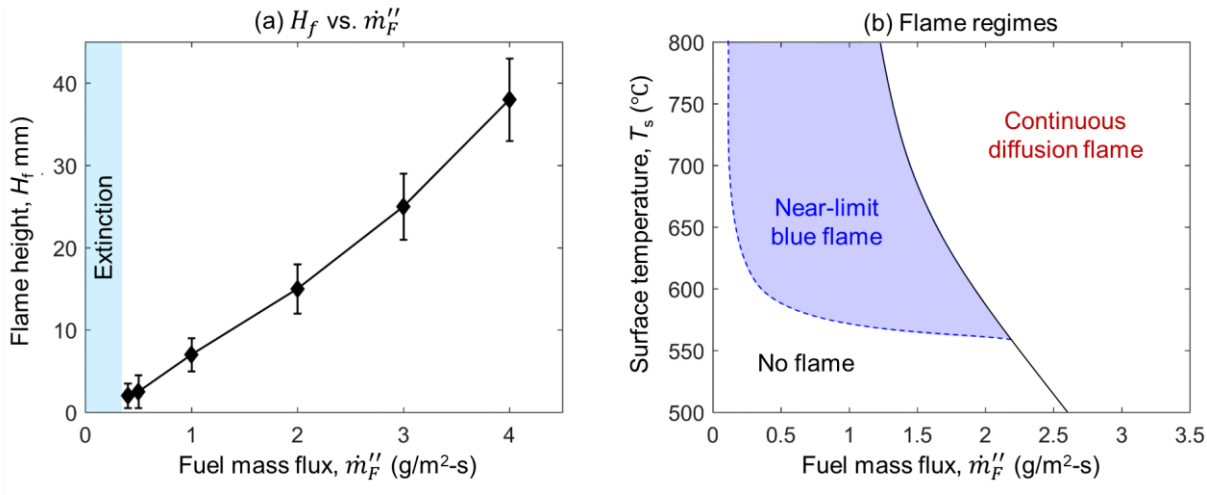

Fig. 7. (a) Modeled average flame height as a function of $\dot{m}''_F$, where for $\dot{m}''_F > 3$ g/m²·s, a larger computational domain is used, and the error bar shows the fluctuation of the flame peak; and (b) modeled different flame regimes.

Therefore, different flame regimes can be obtained by the numerical simulations and summarized as a function of the fuel surface temperature and gaseous fuel mass flux in Fig. 7(b). The continuous diffusion flame region is defined if only one flame peak is observed. Essentially, there is a minimum surface temperature of about 550 ℃ and a minimum mass flux of about 0.3 g/m²·s for the occurrence of the discrete near-limit surface flame. Such behaviors qualitatively agree with the experimental observations [3].

Modeling results further show that by increasing the activation energy (E) of the flame chemistry and mixing CO_2 with the fuel gas, the minimum surface temperature for the near-limit flame behavior will increase. However, because of the limited knowledge about fuel gas composition and flame chemistry, these values are not manually tuned to get a qualitative agreement with the experiment. Also, without the detailed chemistry for flame and soot, the reason for the blue color of flame observed in the experiment cannot be fully revealed based on the current model, which could be explored with a more comprehensive model in future work.

4. Conclusions

In this work, we applied two numerical models to explain the combustion mechanisms responsible for the near-limit blue flame observed in our previous experimental work. Simulation results verify two hypotheses for such a near-limit flame, (1) weak pyrolysis sustained by smoldering in-depth, and (2) hot surface temperature maintained by strong irradiation. The solid-phase model first successfully predicts the mass burning rate of the wood during flaming and smoldering process. Also, it demonstrates that the gaseous fuels for the near-limit blue flame are mainly supplied from the pyrolysis reaction (mainly lignin). The pyrolysis of lignin is maintained by internal smoldering combustion together with strong external radiation.

On the other hand, the gas-phase model demonstrates the necessity of a hot surface and a critical mass flux to main a near-limit flame. Such a near-limit flame is relatively weak that is only slightly affected by buoyancy. The minimum temperature to maintain that flame is 600 ℃, and the required minimum fuel mass flux decreases, as the top surface temperature increases. Finally, different flame regimes are obtained by the numerical simulations and summarized as a function of the fuel surface temperature and gaseous fuel mass flux. The future work will focus on emission gas compositions from different combustion stages, as well as numerical simulations coupling gas-phase and solid-phase processes. This newly observed blue flame may play an essential role in the transition between flaming and smoldering and help evaluate the fire risk of timber under real fire scenarios.

Declaration of Competing Interest

The authors declare that there is no conflict of interest.

Acknowledgements

This work is supported by the National Natural Science Foundation of China (No. 51876183).

References

1. Richter F, Atreya A, Kotsovinos P, Rein G (2019) The effect of chemical composition on the charring of wood across scales. Proc Combust Inst 37:4053–4061. https://doi.org/10.1016/j.proci.2018.06.080
2. Barber D (2015) Tall Timber Buildings: What's Next in Fire Safety ? Fire Technol 51:1279–1284. https://doi.org/10.1007/s10694-015-0497-7
3. Lin S, Huang X, Gao J, Ji J (2022) Extinction of wood fire: A near-limit blue flame above smoldering surface. Fire Technol 58:415–434. https://doi.org/10.1007/s10694-021-01146-6
4. Vermesi I, Richter F, Chaos M, Rein G (2020) Ignition and Burning of Fibreboard Exposed to Transient Irradiation. Fire Technol. https://doi.org/10.1007/s10694-020-01017-6
5. Boonmee N, Quintiere JG (2005) Glowing ignition of wood: The onset of surface combustion. Proc Combust Inst 30 II:2303–2310. https://doi.org/10.1016/j.proci.2004.07.022
6. McAllister S, Finney M (2017) Autoignition of wood under combined convective and radiative heating. Proc Combust Inst 36:3073–3080. https://doi.org/10.1016/j.proci.2016.06.110
7. Babrauskas V (2002) Ignition of Wood : A Review of the State of the Art. J Fire Prot Eng 12:163–189. https://doi.org/10.1106/104239102028711
8. Simms DL (1963) On the pilot ignition of wood by radiation. Combust Flame 7:253–261. https://doi.org/10.1016/0010-2180(63)90190-1
9. Bartlett AI, Hadden RM, Bisby LA (2019) A Review of Factors Affecting the Burning Behaviour of Wood for Application to Tall Timber Construction. Fire Technol 55:1–49. https://doi.org/10.1007/s10694-018-0787-y
10. Janssens M (1991) Piloted Ignition of Wood: A Review. Fire Mater 15:151–167. https://doi.org/10.1002/fam.810150402

11. Emberley R, Do T, Yim J, Torero JL (2017) Critical heat flux and mass loss rate for extinction of flaming combustion of timber. Fire Saf J 91:252–258. https://doi.org/10.1016/j.firesaf.2017.03.008
12. Wang S, Ding P, Lin S, et al (2021) Smoldering and Flaming of Disc Wood Particles Under External Radiation: Autoignition and Size Effect. Front Mech Eng 7:1–11. https://doi.org/10.3389/fmech.2021.686638
13. Cuevas J, Torero JL, Maluk C (2020) Flame extinction and burning behaviour of timber under varied oxygen concentrations. Fire Saf J 103087. https://doi.org/10.1016/j.firesaf.2020.103087
14. Emberley R, Inghelbrecht A, Yu Z, Torero JL (2017) Self-extinction of timber. Proc Combust Inst 36:3055–3062. https://doi.org/10.1016/j.proci.2016.07.077
15. Bartlett AI, Hadden RM, Hidalgo JP, et al (2017) Auto-extinction of engineered timber: Application to compartment fires with exposed timber surfaces. Fire Saf J 91:407–413. https://doi.org/10.1016/j.firesaf.2017.03.050
16. Quintiere J (1997) Principles of Fire Behaviour. Alar Elken, New York
17. Yamazaki T, Matsuoka T, Nakamura Y (2019) Near-extinction behavior of smoldering combustion under highly vacuumed environment. Proc Combust Inst 37:4083–4090. https://doi.org/10.1016/j.proci.2018.06.200
18. Huang X, Gao J (2020) A review of near-limit opposed fire spread. Fire Saf J 103141. https://doi.org/10.1016/j.firesaf.2020.103141
19. Li K, Huang X, Fleischmann C, et al (2014) Pyrolysis of Medium-Density Fiberboard : Optimized Search for Kinetics Scheme and Parameters via a Genetic Algorithm Driven by Kissinger's Method. Energy & Fuels 28:6130−6139. https://doi.org/10.1021/ef501380c
20. Wang S, Ding P, Lin S, et al (2021) Deformation of wood slice in fire: Interactions between heterogeneous chemistry and thermomechanical stress. Proc Combust Inst 38:5081–5090. https://doi.org/10.1016/j.proci.2020.08.060
21. Huang X, Li K, Zhang H (2017) Modelling bench-scale fire on engineered wood : Effects of transient flame and physicochemical properties. Proc Combust Inst 36:3167–3175. https://doi.org/10.1016/j.proci.2016.06.109
22. Moallemi MK, Zhang H, Kumar S (1993) Numerical modeling of two-dimensional smoldering processes. Combust Flame 95:170–182. https://doi.org/10.1016/0010-2180(93)90059-C
23. Kallada Janardhan R, Hostikka S (2019) Predictive Computational Fluid Dynamics Simulation of Fire Spread on Wood Cribs. Fire Technol 55:2245–2268. https://doi.org/10.1007/s10694-019-00855-3
24. Slopiecka K, Bartocci P, Fantozzi F (2012) Thermogravimetric analysis and kinetic study of poplar wood pyrolysis. Appl Energy 97:491–497. https://doi.org/10.1016/j.apenergy.2011.12.056
25. Richter F, Jervis FX, Huang X, Rein G (2021) Effect of oxygen on the burning rate of wood. Combust Flame 234:111591. https://doi.org/10.1016/j.combustflame.2021.111591
26. Shen DK, Fang MX, Luo ZY, Cen KF (2007) Modeling pyrolysis of wet wood under external heat flux. Fire Saf J 42:210–217. https://doi.org/10.1016/j.firesaf.2006.09.001
27. Lautenberger C (2016) Gpyro-A Generalized Pyrolysis Model for Combustible Solids: Users'Guide.

Berkeley

28. Huang X, Rein G (2016) Thermochemical conversion of biomass in smouldering combustion across scales: The roles of heterogeneous kinetics, oxygen and transport phenomena. Bioresour Technol 207:409–421. https://doi.org/10.1016/j.biortech.2016.01.027
29. Richter F, Rein G (2020) A multiscale model of wood pyrolysis to study the role of chemistry and heat transfer at the mesoscale. Combust Flame 216:316–325. https://doi.org/10.1016/j.combustflame.2020.02.029
30. Huang X, Rein G (2014) Smouldering combustion of peat in wildfires: Inverse modelling of the drying and the thermal and oxidative decomposition kinetics. Combust Flame 161:1633–1644. https://doi.org/10.1016/j.combustflame.2013.12.013
31. Huang X, Rein G (2019) Upward-and-downward spread of smoldering peat fire. Proc Combust Inst 37:4025–4033. https://doi.org/10.1016/j.proci.2018.05.125
32. Lin S, Yuan H, Huang X (2022) A Computational Study on the Quenching and Near-Limit Propagation of Smoldering Combustion. Combust Flame 238:. https://doi.org/10.1016/j.combustflame.2021.111937
33. Lautenberger C, Fernandez-Pello C (2009) A model for the oxidative pyrolysis of wood. Combust Flame 156:1503–1513. https://doi.org/10.1016/j.combustflame.2009.04.001
34. Amaral SS, de Carvalho Junior JA, Costa MAM, et al (2014) Comparative study for hardwood and softwood forest biomass: Chemical characterization, combustion phases and gas and particulate matter emissions. Bioresour Technol 164:55–63. https://doi.org/https://doi.org/10.1016/j.biortech.2014.04.060
35. McGrattan K, Hostikka S, McDermott R, et al (2013) Fire dynamics simulator technical reference guide volume 1: mathematical model. NIST Spec Publ 1018:175
36. Gauthier G, Melkior T, Grateau M, et al (2013) Pyrolysis of centimetre-scale wood particles: New experimental developments and results. J Anal Appl Pyrolysis 104:521–530. https://doi.org/10.1016/j.jaap.2013.05.017
37. Yang H, Yan R, Chen H, et al (2007) Characteristics of hemicellulose, cellulose and lignin pyrolysis. Fuel 86:1781–1788. https://doi.org/10.1016/j.fuel.2006.12.013
38. Fereres S, Lautenberger C, Fernandez-Pello AC, et al (2012) Understanding ambient pressure effects on piloted ignition through numerical modeling. Combust Flame 159:3544–3553. https://doi.org/10.1016/j.combustflame.2012.08.006
39. Lautenberger C, Fernandez-Pello C (2009) Generalized pyrolysis model for combustible solids. Fire Saf J 44:819–839. https://doi.org/10.1016/j.firesaf.2009.03.011

Appendix

Fig. A1 compares the experimental and modeling TGA data of wood used in our previous work [3] under (a) non-oxidative nitrogen ambient, and (b) air with 20.9% oxygen at the heating rate of 10 and 50 K/min, and the modeled reaction profiles at 50 K/min are also shown in (c) and (d), respectively. In general, a good agreement is demonstrated for TGA data under different heating rates, especially for the pure pyrolysis process. Without oxidative pyrolysis (Fig. A1a and c), hemicellulose and cellulose will be completely decomposed before about 350 ℃ and 400 ℃, respectively. The decomposition of lignin is much more difficult, which cannot be completely decomposed even at 700 ℃. Meanwhile, with oxygen, the pyrolysis of hemicellulose and cellulose occurs at a lower temperature, and the char oxidation dominates in the mass loss above 400 ℃, coinciding with pyrolysis of lignin.

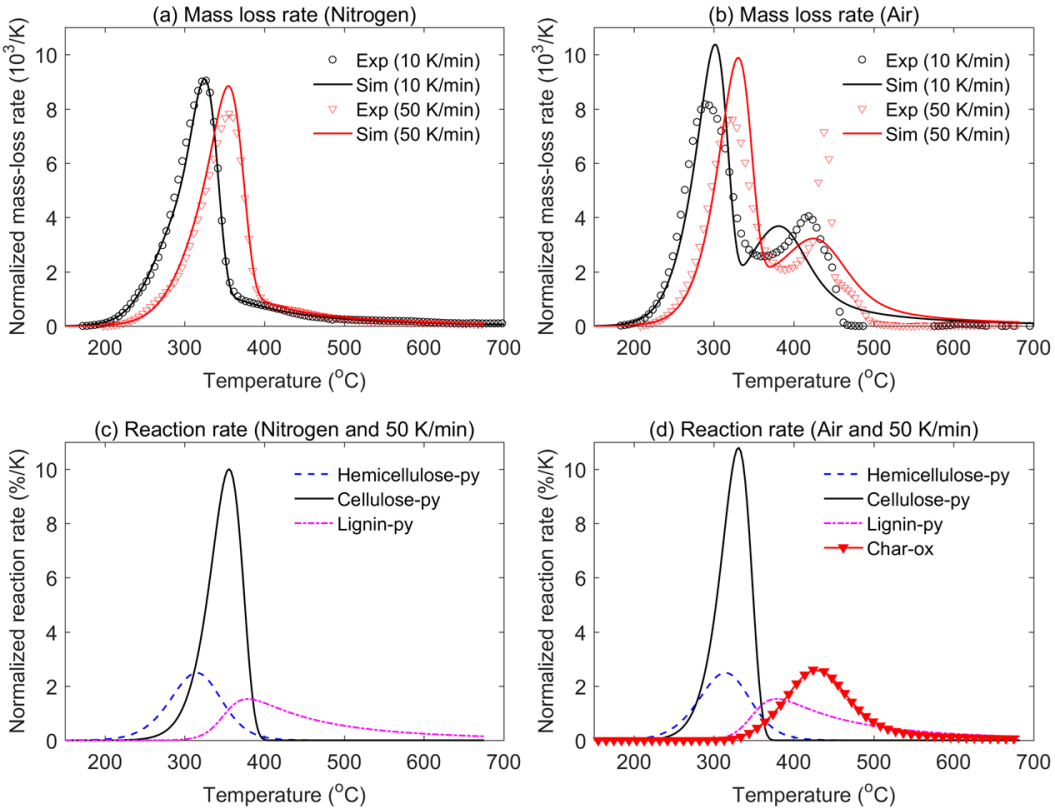

Fig. A1. (a-b) Measured and predicted mass-loss rate curves for the thermal analysis of Wood used in [3], and (c-d) the predicted reaction rate profiles of the smoldering wood by a 4-step smoldering kinetic scheme.